

## Experimental studies of the quantum chromodynamics phase diagram at the STAR experiment

LOKESH KUMAR<sup>1,2,\*</sup> and DECLAN KEANE<sup>3</sup>

<sup>1</sup>School of Physical Sciences, National Institute of Science Education and Research, Bhubaneswar 751 005, India

<sup>2</sup>Department of Physics, Panjab University, Chandigarh 160 014, India

<sup>3</sup>Department of Physics, Kent State University, Kent, Ohio 44242, USA

\*Corresponding author. E-mail: lokesh@pu.ac.in

DOI: 10.1007/s12043-015-0969-9; ePublication: 6 May 2015

**Abstract.** We review the STAR experiment's results to date from the Beam Energy Scan (BES) at Brookhaven's Relativistic Heavy Ion Collider, and outline future plans and prospects in this area. BES Phase-I is based on Au + Au data taken in 2010 and 2011 at  $\sqrt{s_{NN}} = 7.7, 11.5, 19.6, 27$  and  $39$  GeV, and when interpreted in conjunction with the large datasets available at  $62.4$  and  $200$  GeV, permits an initial exploration of the phase diagram of quantum chromodynamics (QCD) matter. The three goals of BES Phase-I are as follows: (1) a search for turn-off of the promising signatures of quark gluon plasma (QGP) already reported at the top RHIC energies; (2) a search for evidence of a possible first-order phase transition such as a signature of softening of the QCD equation of state (EoS); (3) a search for a critical end point as expected in a scenario where there is a cross-over transition from hadronic matter to QGP at the highest RHIC energies, but a first-order phase transition at lower energies with finite net-baryon density. We summarize several analyses of BES data from 2010 and 2011 that are either published or submitted, as well as several more that have been reported at meetings in preliminary forms. The physics interpretation of BES Phase-I measurements is frequently limited by the increasing statistical error bars as the beam energy decreases, and the planned BES Phase-II will have much improved capabilities in this regard.

**Keywords.** Quark gluon plasma; quantum chromodynamics phase diagram; quantum chromodynamics critical point; phase transition; chemical freeze-out; directed and elliptic flow; chiral magnetic effect; nuclear modification factor.

PACS Nos 25.75.-q; 25.75.Nq; 12.38.Mh; 25.75.Dw; 25.75.Gz; 25.75.Ld

### 1. Introduction

Experiments to date at the Relativistic Heavy-Ion Collider (RHIC) at Brookhaven National Laboratory have uncovered evidence for production of a deconfined partonic phase – quark gluon plasma (QGP) – in Au+Au collisions at top RHIC energies [1–5].

However, questions remain about how nuclear matter undergoes the transition from its initial state to a deconfined QGP and then back to a hot hadronic gas. Our current level of understanding is illustrated by the conceptual phase diagram in figure 1. The transition is believed to be a smooth cross-over [6–8] at top RHIC energies. By colliding at progressively lower energies, it should be possible to traverse regions of increasingly high baryon chemical potential  $\mu_B$ , offering the possibility to explore the hypothesized first-order phase transition [9,10] and the vicinity of the associated critical point.

In this review paper, we focus on a dedicated programme at RHIC called the beam energy scan (BES), whose three goals are given in the abstract. Two main phases are predicted in the QCD phase diagram: QGP and hadronic gas. The end-point of the first-order phase transition line (while going towards the cross-over) is the position of a critical point [11]. While there is little guidance from the theory side about the QCD phase diagram, efforts are going on from the experimental side to establish some of its distinct structures, such as the phase boundary between the deconfined phase of quarks and gluons and the hadron gas phase, the first-order phase transition line, and the critical point.

The QCD phase diagram can be studied by inferring the location of a particular experimental dataset along the two axes,  $T$  and  $\mu_B$ . These quantities can be obtained from the momentum distributions and the ratios of the produced particles. Each beam energy point corresponds to one  $T-\mu_B$  coordinate pair on the phase diagram. Data at different centre-of-mass energies can be collected, and once the  $T-\mu_B$  coordinates are inferred from a model-dependent calculation, the various signatures for the phase boundary, first-order phase transition, and critical point can be investigated. One promising approach is to note the beam energy where the signatures of QGP, already established at the top RHIC energy,

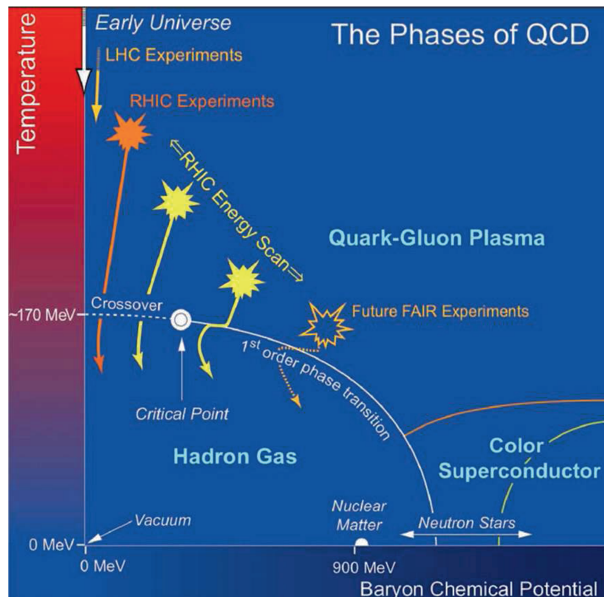


**Figure 1.** Schematic QCD phase diagram, plotted as temperature  $T$  vs. baryon chemical potential  $\mu_B$ .

**Table 1.** Summary of data collected during BES-I, currently proposed energies, corresponding  $\mu_B$  values, event rates, and the required number of events for BES Phase-II. Also listed are the corresponding fixed target  $\sqrt{s_{NN}}$ , number of events, and  $\mu_B$  reach.

Collider energies					Fixed target collisions		
$\sqrt{s_{NN}}$ (GeV)	$\mu_B$ (MeV)	BES-I Evts (M)	Rate $\left(\frac{\text{MEvts}}{\text{day}}\right)$	BES-II Evts (M)	$\sqrt{s_{NN}}$ (GeV)	Evts (M)	$\mu_B$ (MeV)
39	115	130	20	—	—	—	—
27	155	70	9	—	—	—	—
19.6	205	36	3.6	400	4.5	5	585
14.5	250	—	1.6	100	4.0	5	620
11.5	315	12	1.1	120	3.5	5	670
7.7	420	4.3	0.5	80	3.0	5	720

disappear or ‘turn-off’. This is the above-mentioned first goal of the RHIC beam energy scan programme [12–14].

The proposal for the BES programme was given in 2008. This was followed the same year by successful data taking and a physics analysis of a short Au+Au test run at  $\sqrt{s_{NN}} = 9.2$  GeV [15]. The first phase of the BES programme was conducted in the year 2010, with data taking for Au+Au collisions at the three energies of 7.7, 11.5, and 39 GeV. In the year 2011, two additional energy points were added:  $\sqrt{s_{NN}} = 19.6$  and 27 GeV. Table 1 lists various energies and the corresponding number of events collected by the STAR detector in 2010–2011 for Phase-I of the BES programme.

This article is organized as follows. In §2, freeze-out parameters that provide information about  $T$ – $\mu_B$  points in the QCD phase diagram are discussed. Subsequent sections cover signatures of a possible first-order phase transition and the topic of ‘turn-off’ of QGP. Signatures of a possible critical point are then discussed. The last section before the summary addresses the plans and outlook for the BES Phase-II programme.

## 2. Freeze-out parameters

The QCD phase diagram shows the region of each phase in the space of temperature  $T$  and baryon chemical potential  $\mu_B$ . These quantities can be extracted from the measured hadron yields. Transverse momentum  $p_T$  spectra for the BES Phase-I energies are obtained for  $\pi$ ,  $K$ ,  $p$ ,  $\Lambda$ ,  $\Xi$ ,  $K_S^0$ , and  $\phi$  [16,17]. From these distributions, the corresponding particle yields are obtained and various particle ratios are constructed. These particle ratios are used to obtain the chemical freeze-out conditions (at which point, particle yields are no longer able to change), using the statistical thermal model (THERMUS) [2,18,19]. The two main extracted parameters are chemical freeze-out temperature  $T_{ch}$  and  $\mu_B$ . Figure 2 shows the variation of the extracted chemical freeze-out parameters using the grand-canonical ensemble (GCE) approach of THERMUS for different energies and centralities [20,21]. The curves represent the parametrizations of  $T$  and  $\mu_B$  [22,23]. We observe that at top RHIC energy, there is little variation of chemical freeze-out parameters

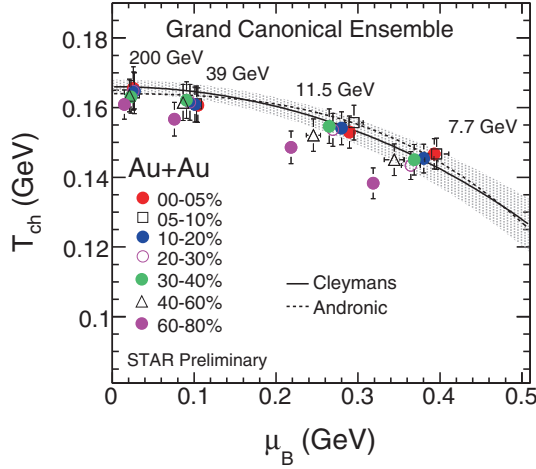


**Figure 2.** Variation of  $T_{ch}$  with  $\mu_B$  for different energies and centralities. The curves represent theoretical calculations [22,23].

with centrality, while at lower energies,  $T_{ch}$  shows a variation with  $\mu_B$  as a function of centrality. The centrality dependence of these parameters is observed for the first time in heavy-ion collisions at these lower energies. One advantage of having such a dependence is that experiments can explore a larger region of the QCD phase diagram without as many changes in beam energy as might otherwise be needed, allowing collider beam time to be utilized more efficiently.

### 3. Directed flow

The directed flow  $v_1$  is calculated as  $\langle \cos(\phi - \Psi_1) \rangle$ , where  $\phi$  and  $\Psi_1$  are the azimuthal angle of the produced particles and the azimuthal orientation of the first-order reaction plane, respectively. The directed flow measurements for protons are proposed to be sensitive to the equation of state (EoS) [24–27]. Based on a 3-fluid hydrodynamic model with a first-order phase transition from hadronic matter to QGP, it has been specifically predicted that proton  $v_1(y)$  slope should exhibit a sharp minimum as a function of beam energy [26,27], whereas the same model with a purely hadronic EoS predicts monotonic behaviour. The Frankfurt theory group refers to the QGP EoS behaviour as a collapse of proton flow. Figure 3 shows directed flow results from the beam energy scan. In figure 3, the  $v_1$  slope  $dv_1/dy$  near midrapidity is plotted as a function of beam energy for mid-central (10–40%) Au+Au collisions, for antiprotons, protons, and net protons [29,30]. The antiproton slope increases with increasing collision energy but stays below zero up to 200 GeV. The proton slope decreases strongly with energy and changes sign from positive to negative between 7.7 and 11.5 GeV, shows a minimum between 11.5 and 19.6 GeV, and remains small but negative up to 200 GeV. The  $v_1(y)$  slope for net-protons is negligibly different from protons at and below the energy of the minimum, but then crosses zero between 27 GeV and 39 GeV, and remains positive up to 200 GeV. The UrQMD model does not reproduce the behaviour shown in the data. The observed beam energy of the



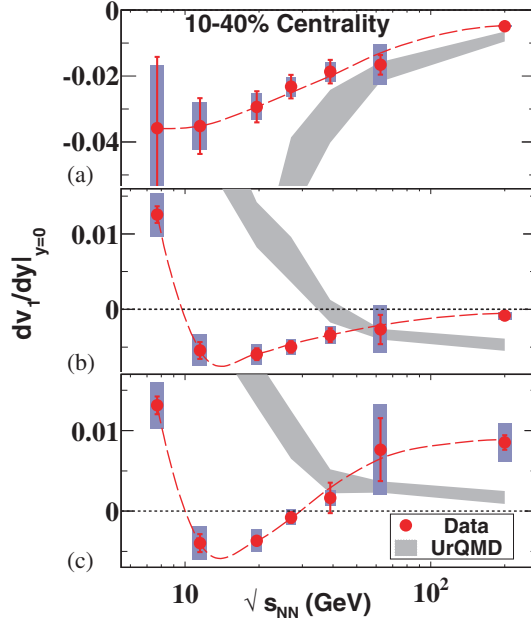


**Figure 3.** Directed flow slope ( $dv_1/dy$ ) near midrapidity as a function of beam energy for intermediate-centrality (10–40%) Au+Au collisions. Panels (a), (b), and (c) report STAR’s measurement for antiprotons, protons, and net protons, respectively, along with the corresponding calculations from the UrQMD hadronic transport model [28] subject to the same cuts and fit conditions. The systematic uncertainties on the measurements are shown as shaded bars. The dashed curves are a smooth fit to guide the eye.

minimum in  $v_1(y)$  slope for both protons and net protons in the data is a factor of 3 to 4 higher than the minimum in the hydrodynamic prediction with a QGP EoS having a first-order phase transition [27]. At the energy where the hydrodynamic model predicts a minimum, and at the higher energy where a minimum is observed by STAR, the difference between all the protons and net protons is negligible.

In order to refine the minimum position, it will be very valuable to add one more energy point around 15 GeV, and additional statistics would allow centrality dependence to be explored. Also, more theoretical studies are needed to fully understand these interesting observations, and to definitively rule out possible explanations based on purely hadronic physics.

#### 4. Elliptic flow

The elliptic flow  $v_2$  is defined in terms of  $\langle \cos 2(\phi - \Psi_2) \rangle$ , where  $\Psi_2$  is the orientation of the second-order reaction plane. Like directed flow, elliptic flow mainly probes the early stages of heavy-ion collisions. In Au+Au collisions at the top RHIC energy of 200 GeV, the elliptic flow vs.  $m_T - m_0$  (where  $m_T = \sqrt{p_T^2 + m_0^2}$ ) for mesons and baryons

show separation at intermediate  $p_T$ . However, when both axes are scaled by the number of constituent quarks ( $n_q$ ),  $v_2$  shows a scaling behaviour where mesons and baryons almost coincide over a range of  $p_T$  values. This is referred to as the number of constituent quark (NCQ) scaling [31]. It is a widely accepted signature of partonic matter formed in Au+Au collisions at 200 GeV [1,2], and deviations from such scaling might indicate a return to dominance by hadronic interactions. Hence, breaking of NCQ scaling at lower energies could be an indication of a ‘turn-off’ of QGP production. For NCQ scaling to happen,  $v_2$  of mesons and baryons must show splitting or separation at intermediate  $p_T$ . Absence of such a splitting could also be taken as an indication of ‘turn-off’ of QGP. Figure 4 shows the difference in  $v_2$  of particles and the corresponding antiparticles as a function of beam energy [32]. The difference in  $v_2$  between particles and antiparticles is observed to increase as the energy is lowered. At low energies,  $v_2(\pi^-) > v_2(\pi^+)$ ,  $v_2(K^+) > v_2(K^-)$ , and  $v_2(\text{baryons}) > v_2(\text{antibaryons})$ . This difference between particles and antiparticles suggests that the NCQ scaling among particles and antiparticles is broken. However, the observed difference between  $v_2$  of particles and antiparticles could be qualitatively explained by models incorporating baryon transport at midrapidity and hadronic interactions [33,34].

Figure 5 shows  $v_2$  vs.  $m_T - m_0$  for different particle types at  $\sqrt{s_{NN}} = 7.7\text{--}62.4$  GeV, and the splitting into one common curve for mesons and another common curve for baryons can be seen for higher energies [32]. The splitting between baryons and mesons decreases with decreasing beam energy, and disappears around  $\sqrt{s_{NN}} \leq 11.5$  GeV. As the baryon–meson splitting at top RHIC energy is attributed to partonic degrees of freedom, its absence at lower energies suggests that partonic effects are less dominant at lower energies. In addition, it is also observed that all particle types, both mesons and baryons, when scaled by the corresponding number of quarks (two for mesons and three for baryons), follow a single common curve within about  $\pm 10\%$ , except for  $\phi$ -mesons at  $\sqrt{s_{NN}} \leq 11.5$  GeV [32]. At the largest  $m_T - m_0$ , the  $\phi$ -meson datapoints deviate by  $1.8\sigma$  and  $2.3\sigma$  for  $\sqrt{s_{NN}} = 7.7$  and 11.5 GeV, respectively. As  $\phi$ -mesons have a smaller hadronic interaction

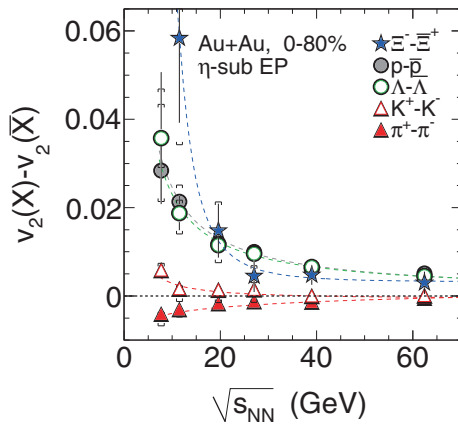


**Figure 4.** The difference in  $v_2$  between particles and their corresponding antiparticles as a function of beam energy in 0–80% Au+Au collisions. Both statistical (vertical lines) and systematic errors (caps) are shown.

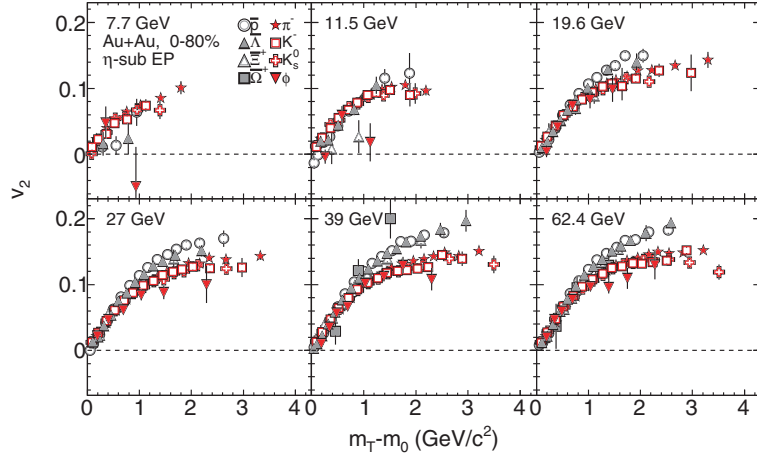


**Figure 5.**  $v_2$  as a function of  $m_T - m_0$  for different particle types in Au+Au collisions at  $\sqrt{s_{NN}} = 7.7, 11.5, 19.6, 27, 39,$  and  $62.4$  GeV. The errors shown are statistical only.

cross-section, their smaller  $v_2$  could indicate that the hadronic interactions start to dominate over partonic effects for systems formed at beam energies  $\sqrt{s_{NN}} \leq 11.5$  GeV [35]. However, much higher statistics are needed to extend the  $m_T - m_0$  range of  $\phi$ -mesons and improve the significance of the observed deviation.

## 5. Chiral magnetic effect

In non-central heavy-ion collisions, a large orbital angular momentum vector ( $L$ ) exists at  $90^\circ$  to the reaction plane, leading to an exceptionally intense localized magnetic field ( $\sim 10^{15}$  T). If the system is deconfined, there can be strong parity-violating domains, and different numbers of quarks of left- and right-handed helicity, leading to preferential emission of like-sign charged particles along  $L$ . The phenomenon is sometimes called the chiral magnetic effect (CME) [36–38], and has been studied in lattice QCD [39–41]. Experimentally, such a phenomenon could be studied through a three-particle mixed-harmonic azimuthal correlator [42,43],  $\gamma = \langle \cos(\phi_\alpha + \phi_\beta - 2\Psi_{RP}) \rangle$ . This observable represents the difference between azimuthal correlations projected onto the direction of the angular momentum vector and correlations projected onto the collision reaction plane. At top RHIC energies, the correlator  $\gamma$  shows a separation between the correlations of same- and opposite-sign charges with respect to the reaction plane [42,43]. These results are consistent with the expected signal for local parity violation, especially the centrality dependence. However, there are caveats attached to this observation [42–44]. If this difference can be attributed to the QCD phase transition, the absence of such an observation at lower energies could be an indication that the system did not undergo the phase transition. Hence, the observable could be useful to locate the beam energy where the QGP signature ‘turns off’.

Figure 6 shows the correlator  $\gamma$  as a function of centrality from Au+Au collisions at  $\sqrt{s_{NN}} = 7.7$ –200 GeV [45]. For comparison, we also show the ALICE results for Pb+Pb

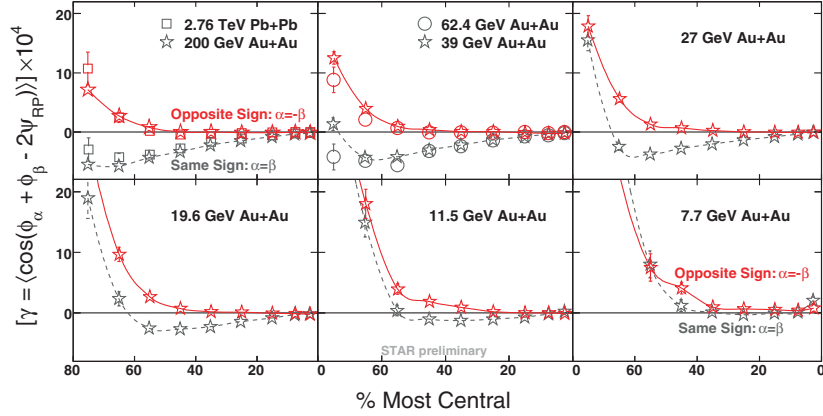


**Figure 6.** The correlator  $\gamma$  as a function of centrality for Au+Au collisions from 200 GeV to 7.7 GeV. For comparison, we also show ALICE results for Pb+Pb at 2.76 TeV [46]. The plotted errors are statistical only.

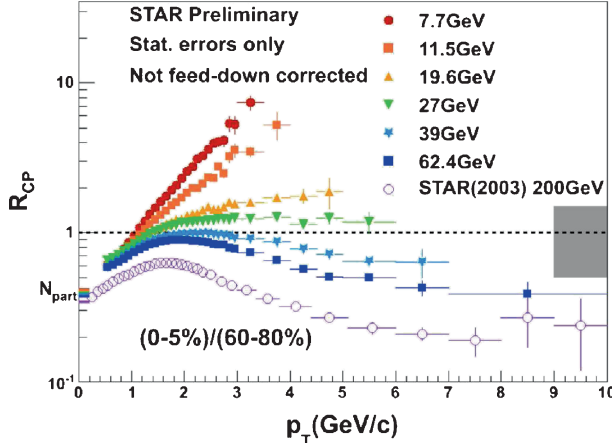
collisions at 2.76 TeV [46]. As can be seen in figure 6, the  $\gamma$  signals are very similar in collisions throughout the beam energy range  $\sqrt{s_{NN}} = 2.76$  TeV down to 19.6 GeV. However, changes in the correlation function are seen at lower energies:  $\sqrt{s_{NN}} = 11.5$  and 7.7 GeV, where the difference between same-sign and opposite-sign  $\gamma$  fades away at all collision centralities. As discussed above, one possible explanation for this fading away would be the disappearance of CME due to a turn-off of deconfinement at lower BES energy points.

## 6. Nuclear modification factor

The behaviour of the nuclear modification factor  $R_{CP}$  is a widely accepted signature of QGP at top RHIC energy [47]. This observable is defined as the ratio of yields in central collisions to yields in peripheral collisions, scaled by the corresponding number of binary collisions  $N_{bin}$ . The number of binary collisions is calculated from a Monte Carlo model. At high  $p_T$ , it has been observed that  $R_{CP}$  of various particles is less than unity [47], which is attributed to energy loss of the partons in the dense medium. In the absence of a dense medium, there may not be suppression of high  $p_T$  particles, which might serve as an indication of ‘turn-off’ of QGP production.

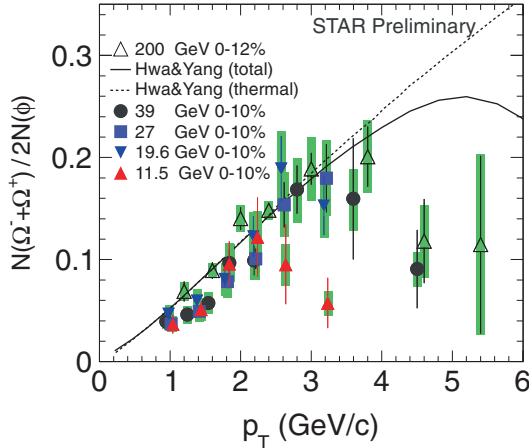
Figure 7 shows  $R_{CP}$  results for charged hadrons in Au+Au collisions at  $\sqrt{s_{NN}} = 7.7$ –200 GeV [48]. We observed that for  $p_T > 2$  GeV/c,  $R_{CP} > 1$  for lower energies. This suggests that partonic effects become less important and the cold nuclear matter effects (Cronin effect) start to dominate at these lower energies [49]. A caveat is that, as the hard spectrum component fades away with decreasing beam energy, disentangling the various factors as the beam energy is scanned down remains a challenge to be solved in future.

Figure 8 shows the baryon-to-meson ratio  $N(\Omega^- + \Omega^+)/2N(\phi)$  as a function of  $p_T$  in central Au+Au collisions at  $\sqrt{s_{NN}} = 11.5$ –200 GeV [50]. The curves represent model calculations by Hwa and Yang [51,52] in central collisions at  $\sqrt{s_{NN}} = 200$  GeV which assume the  $\Omega$  and  $\phi$  yields to be generated from the recombination of thermal strange



**Figure 7.**  $R_{CP}((0-5\%)/(60-80\%))$  for charged hadrons in Au+Au collisions at  $\sqrt{s_{NN}} = 7.7-200$  GeV. The grey band at the right corresponds to systematic uncertainties.

quarks having an exponential  $p_T$  distribution. The particle ratio results at  $\sqrt{s_{NN}} = 19.6$ , 27, and 39 GeV seem to be consistent with 200 GeV results, indicating a maximum around  $p_T \geq 3$  GeV/c, then turning down as  $p_T$  increases further. However, results at 11.5 GeV suggest a different behaviour, i.e., they show a maximum at the somewhat lower  $p_T$  of  $\sim 2$  GeV/c before turning down at higher  $p_T$ . This observation suggests that there might be a change in the underlying  $p_T$  distributions of strange quarks recombining to form the final  $\Omega$  and  $\phi$  for  $\sqrt{s_{NN}} = 11.5$  GeV, compared with  $\sqrt{s_{NN}} \geq 19.6$  GeV. This is another good example of a measurement where the expected roughly ten-fold increase in statistics in BES Phase-II could allow a major step forward.



**Figure 8.** The baryon-to-meson ratio  $N(\Omega^- + \Omega^+)/2N(\phi)$  as a function of  $p_T$  in central Au+Au collisions at  $\sqrt{s_{NN}} = 11.5-200$  GeV. The curves are from model calculations by Hwa and Yang for  $\sqrt{s_{NN}} = 200$  GeV. Both statistical errors (vertical lines) and systematic errors (shaded bands) are shown.

## 7. Conserved number fluctuations

Higher moments of conserved number fluctuations have been proposed as promising observables in the search for a critical point [53–55]. For a static, infinite medium, the correlation length  $\xi$  diverges at a critical point. The various moments of event-by-event conserved numbers (such as net baryons, net charge, and net strangeness) are related to different powers of the correlation length. Higher moments such as skewness  $S$  and kurtosis  $\kappa$  are related to higher powers of the correlation length [56,57]. Thus, these higher moments have a better sensitivity in searching for the critical point. It has been proposed that the appropriate products of these moments, such as  $\kappa\sigma^2$  and  $S\sigma$ , can be related to the ratios of order susceptibilities calculated in lattice QCD and HRG models as  $\kappa\sigma^2 = \chi_B^{(4)}/\chi_B^{(2)}$  and  $S\sigma = \chi_B^{(3)}/\chi_B^{(2)}$  [58,59]. Here,  $\chi_B^{(2)}$ ,  $\chi_B^{(3)}$ , and  $\chi_B^{(4)}$  are the second-, third-, and fourth-order baryon number susceptibilities, respectively. One of the advantages of using these products or ratios is that they cancel volume effects which are difficult to estimate in an experiment. In this way, one can relate experimental measurements to lattice QCD observables in searching for a critical point. In an experiment, it

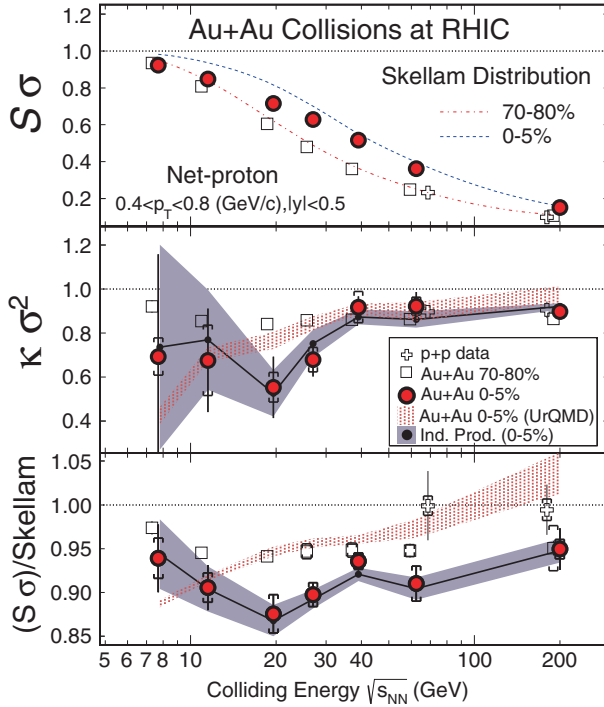


**Figure 9.**  $\kappa\sigma^2$ ,  $S\sigma$ , and  $S\sigma$  values normalized by the Skellam expectations as a function of collision energy and two different centralities. Results from  $p + p$  collisions are also shown. All the results presented are corrected for detector efficiency. One shaded band is an expectation based on assuming independent proton and antiproton production, and the other shaded band is based on the UrQMD model. The widths of the bands represent statistical uncertainties. The error bars on datapoints are statistical while caps represent the systematic errors.

is difficult to measure total baryons on an event-by-event basis, and therefore net protons are used as a proxy for net baryons.

Figure 9 shows  $\kappa\sigma^2$  and  $S\sigma$  for net protons as a function of beam energy for different collision centralities [60,61]. For comparison, results are shown for: (i) Skellam expectations, (ii) expectations based on assuming independent production of protons and antiprotons, and (iii) the UrQMD model, which incorporates much of the relevant physics, but not a critical point [28]. The results from  $p + p$  collisions at 200 GeV are also shown. The bottom panel shows the  $S\sigma$  values normalized by the corresponding Skellam expectations. The moment products  $\kappa\sigma^2$  and  $S\sigma$  show similar values for central (0–5%) and peripheral (70–80%) collisions for  $\sqrt{s_{NN}} = 39$ –200 GeV. For beam energies below 39 GeV, they have different values for central and peripheral collisions. These values are below Skellam expectations for  $\sqrt{s_{NN}} > 7.7$  GeV for 0–5% central collisions, but are described very well at all energies by the expectation based on assuming independent proton and antiproton production. The UrQMD model calculations show a smooth monotonic behaviour as a function of collision energy.

Thus, it is necessary to acquire the much increased statistics of a new Phase-II of the BES programme to continue the search for a critical point. In addition, a direct comparison to QCD calculations with a critical point obtained using similar dynamics as that of heavy-ion collisions is a high priority.

## **8. BES Phase-II**

The first phase of the BES programme has yielded several promising results for understanding the QCD phase diagram. Some of the observables require high statistics data to make definite statements. In addition, the energy dependence of some observables suggests that one more energy point around 15 GeV would be very advantageous. For example, proton and net proton  $v_1$  slopes suggest a minimum as a function of beam energy around 11.5–19.6 GeV, which could be related to the softest point in the equation of state. Similar reasoning might be argued for the freeze-out eccentricity, although there is a monotonic variation as a function of beam energy at this time. For higher moments, adding 14.5 GeV along with high statistics data at lower energies might provide a clear energy dependence trend with high significance. One more energy point at 14.5 GeV is also important in view of the fact that the gap between 11.5 and 19.6 GeV in terms of  $\mu_B$  is more than 100 MeV.

For the reasons mentioned above, Brookhaven National Lab has decided to continue the exploration of the QCD phase diagram and hence a second phase of the BES programme is planned. The proposal for BES Phase-II includes high statistics data below 20 GeV as listed in table 1. To achieve high statistics data at lower energies, electron cooling will be installed at RHIC for increasing the beam luminosity [62]. Additional improvements in luminosity will be possible by operating with longer bunches at the space-charge limit in the collider [63]. Electron cooling may increase the luminosity by a factor of 3–10, and with longer bunches, the luminosity may be increased by another factor of 2–5. The high statistics data from BES Phase-II will allow precision measurements of the important observables discussed here, and will also be helpful in the measurements of rare probes such as dilepton production and hypertriton measurements at lower energies [64,65].



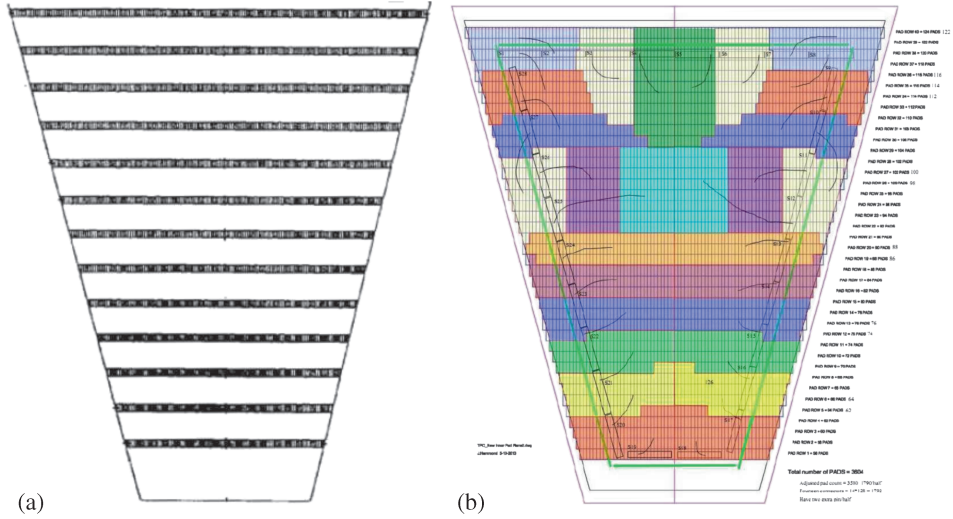


**Figure 10.** (a) Lay-out of the original inner pad plane of the STAR time projection chamber, showing the sparse spatial coverage. (b) The new inner pad plane lay-out, with continuous spatial coverage, proposed for the STAR iTPC upgrade.

To maximize the use of collisions provided at STAR, a fixed-target configuration is under consideration as part of the plan for BES Phase-II. The concept is to install a fixed Au target inside the STAR beam pipe to measure Au (beam) on Au (fixed target) collisions, providing a lower reach for the centre-of-mass energies, and thus a higher reach for the  $\mu_B$  values for a given BES Phase-II energy in each ring. The beam energies and the  $\mu_B$  values for fixed-target collisions are listed in table 1 corresponding to the proposed BES Phase-II collider-mode energies. The  $\mu_B$  values are obtained from the parametrizations in ref. [23]. One of the advantages of such a proposal is that data taking for fixed target collisions can be done concurrently with normal RHIC running in collider mode.

These programmes will also benefit from a proposed inner sector upgrade of the STAR TPC, called the iTPC upgrade [66]. At the moment, inner sector wires of the TPC show signs of ageing, and unlike the outer TPC sectors, they do not have continuous pad coverage at all radii. The spacing between the rows is greater than 5 cm, resulting in missing rows (see figure 10). To overcome these issues, increasing the segmentation and coverage on the inner pad plane, and renewing the inner sector wires has been proposed. Simulation studies indicate that with the iTPC upgrade, it will be possible to improve momentum resolution and  $dE/dx$  resolution for particle identification. Also, there will be improved acceptance at higher pseudorapidity and low  $p_T$ . At the moment, TPC  $\eta$  coverage is about  $|\eta| < 1.0$ , but with the iTPC upgrade,  $|\eta| < 1.7$  is expected. Similarly, the lowest  $p_T$  reached with the iTPC can be as low as 60 MeV/c, compared to the present value of 125 MeV/c. BES Phase-II is expected to start around 2018 or 2019.

## 9. Summary

BES Phase-I enables RHIC to cover a large range of  $\mu_B$  (20–400 MeV) in the QCD phase diagram. At lower energies, a centrality dependence of freeze-out parameters is observed.

Observables such as elliptic flow  $v_2$ , the correlator associated with the chiral magnetic effect, the nuclear modification factor  $R_{CP}$ , and the baryon-to-meson ratio  $\Omega/\phi$ , address the issue of whether hadronic interactions dominate at the lowest energies, with some indications of an answer in the affirmative. The directed flow  $v_1(y)$  slope for protons and net protons shows a minimum between 11.5 and 19.6 GeV that bears a closer resemblance to a model with a first-order phase transition than to a purely hadronic model, but further work in both theory and experiment is needed to clarify the interpretation. The  $\kappa\sigma^2$  and  $S\sigma$  for net protons show deviations from Skellam expectations at some energies but are reproduced by an expectation based on independent proton and antiproton production. BES Phase-II will be enhanced by electron cooling, a planned fixed target, and the iTPC upgrade at STAR. These developments offer an optimistic future for the exploration of the QCD phase diagram.

## References

- [1] S A Bass *et al*, White Paper *Hot & Dense QCD Matter*, submitted to 2012 US Nuclear Science Advisory Committee, [http://www.bnl.gov/npp/docs/Bass\\_RHI\\_WP\\_final.pdf](http://www.bnl.gov/npp/docs/Bass_RHI_WP_final.pdf)
- [2] STAR Collaboration: J Adams *et al*, *Nucl. Phys. A* **757**, 102 (2005)
- [3] PHENIX Collaboration: K Adcox *et al*, *Nucl. Phys. A* **757**, 184 (2005)
- [4] BRAHMS Collaboration: I Arsene *et al*, *Nucl. Phys. A* **757**, 1 (2005)
- [5] PHOBOS Collaboration: B B Back *et al*, *Nucl. Phys. A* **757**, 28 (2005)
- [6] F Karsch *et al*, *Nucl. Phys. Proc. Suppl.* **129**, 614 (2004)
- [7] Y Aoki, G Endroli, Z Fodor, S D Katz and K K Szabo, *Nature* **443**, 675 (2006)
- [8] M Cheng *et al*, *Phys. Rev. D* **79**, 074505 (2009), and references therein
- [9] S Ejiri, *Phys. Rev. D* **78**, 074507 (2008)
- [10] E S Bowman and J I Kapusta, *Phys. Rev. C* **79**, 015202 (2009)
- [11] M A Stephanov, *Prog. Theor. Phys. Suppl.* **153**, 139 (2004); *Int. J. Mod. Phys. A* **20**, 4387 (2005), [hep-ph/0402115]
- [12] STAR Collaboration: M M Aggarwal *et al*, arXiv:1007.2613 (2010)
- [13] STAR Collaboration: L Kumar, *Nucl. Phys. A* **862**, 125 (2011)
- [14] B Mohanty, *Nucl. Phys. A* **830**, 899C (2009)
- [15] STAR Collaboration: B I Abelev *et al*, *Phys. Rev. C* **81**, 024911 (2010)
- [16] STAR Collaboration: L Kumar, *J. Phys. G: Nucl. Part. Phys.* **38**, 124145 (2011)
- [17] STAR Collaboration: X Zhu, *Acta Phys. Polon. B Proc. Suppl.* **5**, 213 (2012)
- [18] A Andronic, F Beutler, P Braun-Munzinger, K Redlich and J Stachel, *Phys. Lett. B* **675**, 312 (2009), arXiv:0804.4132
- [19] S Wheaton and J Cleymans, *Comput. Phys. Commun.* **180**, 84 (2009), hep-ph/0407174
- [20] STAR Collaboration: L Kumar, *Nucl. Phys. A* **904–905**, 256c (2013), arXiv:1211.1350
- [21] STAR Collaboration: S Das, *Nucl. Phys. A* **904–905**, 891c (2013), arXiv:1210.6099
- [22] A Andronic, P Braun-Munzinger and J Stachel, *Nucl. Phys. A* **834**, 237C (2010), arXiv:0911.4931
- [23] J Cleymans, H Oeschler, K Redlich and S Wheaton, *Phys. Rev. C* **73**, 034905 (2006), hep-ph/0511094
- [24] J Brachmann, S Soff, A Dumitru, H Stoecker, J A Maruhn, W Greiner, L V Bravina and D H Rischke, *Phys. Rev. C* **61**, 024909 (2000), nucl-th/9908010
- [25] L P Csernai and D Rohrich, *Phys. Lett. B* **458**, 454 (1999), nucl-th/9908034
- [26] D H Rischke *et al*, *Heavy Ion Phys.* **1**, 309 (1995)
- [27] H Stoecker, *Nucl. Phys. A* **750**, 121 (2005), nucl-th/0406018

- [28] M Bleicher, E Zabrodin, C Spieles, S A Bass, C Ernst, S Soff, L Bravina, M Belkacem *et al*, *J. Phys. G* **25**, 1859 (1999), hep-ph/9909407
- [29] STAR Collaboration: Y Pandit, *Nucl. Phys. A* **904–905**, 357c (2013), arXiv:1210.5315
- [30] STAR Collaboration: L Adamczyk *et al*, arXiv:1401.3043 [nucl-ex]
- [31] STAR Collaboration: J Adams *et al*, *Phys. Rev. Lett.* **95**, 122301 (2005)
- [32] STAR Collaboration: L Adamczyk *et al*, *Phys. Rev. Lett.* **110**, 0142301 (2013)
- [33] J C Dunlop, M A Lisa and P Sorensen, *Phys. Rev. C* **84**, 044914 (2011), arXiv:1107.3078
- [34] J Xu, L-W Chen, C M Ko and Z-W Lin, *Phys. Rev. C* **85**, 041901 (2012), arXiv:1201.3391
- [35] B Mohanty and N Xu, *J. Phys. G* **36**, 064022 (2009)
- [36] D Kharzeev, *Phys. Lett. B* **633**, 260 (2006)
- [37] D E Kharzeev, L D McLerran and H J Warringa, *Nucl. Phys. A* **803**, 227 (2008)
- [38] K Fukushima, D E Kharzeev and H J Warringa, *Phys. Rev. D* **78**, 074033 (2008), arXiv:0808.3382
- [39] P V Buividovich, M N Chernodub, E V Luschevskaya and M I Polikarpov, *Phys. Rev. D* **80**, 054503 (2009)
- [40] M Abramczyk, T Blum, G Petropoulos and R Zhou, *PoS LAT* **2009**, 181 (2009)
- [41] P V Buividovich, E V Lushchevskaya, M I Polikarpov and M N Chernodub, *JETP Lett.* **90**, 412 (2009)
- [42] STAR Collaboration: B I Abelev *et al*, *Phys. Rev. Lett.* **103**, 251601 (2009)
- [43] STAR Collaboration: B I Abelev *et al*, *Phys. Rev. C* **81**, 054908 (2010)
- [44] S Pratt, *Phys. Rev. C* **83**, 014913 (2011)  
S Pratt, S Schlichting and S Gavin, *Phys. Rev. C* **84**, 024909 (2011)
- [45] STAR Collaboration: G Wang, *Nucl. Phys. A* **904–905**, 248c (2013)
- [46] ALICE Collaboration: B Abelev *et al*, *Phys. Rev. Lett.* **110**, 012301 (2013), arXiv:1207.0900
- [47] STAR Collaboration: M A C Lamont, *J. Phys. Conf. Ser.* **50**, 192 (2006)
- [48] STAR Collaboration: E Sangaline, *Nucl. Phys. A* **904–905**, 771c (2013)
- [49] J W Cronin, H J Frisch, M J Shochet, J P Boymond, R Mermod, P A Piroue and R L Sumner, *Phys. Rev. D* **11**, 3105 (1975)
- [50] STAR Collaboration: X Zhang, *Nucl. Phys. A* **904–905**, 543c (2013)
- [51] R C Hwa and C B Yang, *Phys. Rev. C* **75**, 054904 (2007), nucl-th/0602024
- [52] R C Hwa and C B Yang, *Phys. Rev. C* **66**, 025205 (2002), hep-ph/0204289
- [53] STAR Collaboration: M M Aggarwal *et al*, *Phys. Rev. Lett.* **105**, 022302 (2010), arXiv:1004.4959
- [54] S Gupta, X Luo, B Mohanty, H G Ritter and N Xu, *Science* **332**, 1525 (2011), arXiv:1105.3934
- [55] F Karsch and K Redlich, *Phys. Lett. B* **695**, 136 (2011)
- [56] M A Stephanov, *Phys. Rev. Lett.* **102**, 032301 (2009)
- [57] M A Stephanov, *Phys. Rev. Lett.* **107**, 052301 (2011)
- [58] R V Gavai and S Gupta, *Phys. Lett. B* **696**, 459 (2011), arXiv:1001.3796
- [59] M Cheng, P Hendge, C Jung, F Karsch, O Kaczmarek, E Laermann, R D Mawhinney, C Miao, P Petreczky, C Schmidt and W Soeldner, *Phys. Rev. D* **79**, 074505 (2009), arXiv:0811.1006
- [60] STAR Collaboration: X Luo, *Nucl. Phys. A* **904–905**, 911c (2013)
- [61] STAR Collaboration: L Adamczyk *et al*, *Phys. Rev. Lett.* **112**, 032302 (2014), arXiv:1309.5681[nucl-ex]
- [62] A Fedotov and W Fischer, Private communications, 2012
- [63] A Fedotov and M Blaskiewicz, BNL CAD Tech Note: C-A/AP/449 (February 10, 2012)
- [64] STAR Collaboration: B Huang, *Nucl. Phys. A* **904–905**, 565c (2013)
- [65] STAR Collaboration: Y Zhu, *Nucl. Phys. A* **904–905**, 551c (2013)
- [66] STAR Collaboration: Y Xu, poster “Inner TPC Upgrade at STAR”, 2013 RHIC & AGS Annual Users Meeting, BNL, USA